X-ray absorption spectra of hexagonal ice and liquid water by all-electron Gaussian and augmented plane wave calculations

Iannuzzi, Marcella

DOI: https://doi.org/10.1063/1.2928842

X-ray absorption spectra of hexagonal ice and liquid water by all-electron Gaussian and augmented plane wave calculations

Marcella Iannuzzi

Citation: The Journal of Chemical Physics **128**, 204506 (2008); doi: 10.1063/1.2928842
View online: http://dx.doi.org/10.1063/1.2928842
View Table of Contents: http://aip.scitation.org/toc/jcp/128/20
Published by the American Institute of Physics

X-ray absorption spectra of hexagonal ice and liquid water by all-electron Gaussian and augmented plane wave calculations

Marcella Iannuzzi[a)]
Paul Scherrer Institut, CH-5232, Villigen PSI, Switzerland

(Received 14 February 2008; accepted 24 April 2008; published online 27 May 2008)

Full potential x-ray spectroscopy simulations of hexagonal ice and liquid water are performed by means of the newly implemented methodology based on the Gaussian augmented plane waves formalism. The computed spectra obtained within the supercell approach are compared to experimental data. The variations of the spectral distribution determined by the quality of the basis set, the size of the sample, and the choice of the core-hole potential are extensively discussed. The second part of this work is focused on the understanding of the connections between specific configurations of the hydrogen bond network and the corresponding contributions to the x-ray absorption spectrum in liquid water. Our results confirm that asymmetrically coordinated molecules, in particular, those donating only one or no hydrogen bond, are associated with well identified spectral signatures that differ significantly from the ice spectral profile. However, transient local structures, with half formed hydrogen bonds, may still give rise to spectra with dominant postedge contributions and relatively weaker oscillator strengths at lower energy. This explains why by averaging the spectra over all the O atoms of liquid instantaneous configurations extracted from *ab initio* molecular dynamics trajectories, the spectral features indicating the presence of weak or broken hydrogen bonds turn out to be attenuated and sometimes not clearly distinguishable. © *2008 American Institute of Physics*. [DOI: 10.1063/1.2928842]

I. INTRODUCTION

Inner-shell spectroscopy is a powerful structural technique typically used to investigate adsorption processes on metallic surfaces.[1] By highly resolved synchrotron light, individual atoms can be selectively addressed, and the electronic structure is probed locally, to directly resolve the effects of the atomic environment, such as polarization, rehybridization, charge transfer, and formation of covalent bonding. More recently, experimental as well as theoretical studies of hydrogen bonded structures have shown that x-ray absorption spectroscopy (XAS) is suited to identify the presence of hydrogen bonds (H bonds) and to estimate their strength and stability.[2–5]

The technique has been applied to two hydrogen bonded liquids, water, and methanol, where the local conformation around the individual molecules is still a matter of debate. The commonly accepted picture of liquid water is a tetrahedral network of H bonds, through which each molecule is connected to three or four other molecules. This picture has been questioned on the basis of controversial interpretations of experimental XAS and x-ray Raman spectra.[6] Wernet *et al.* compared XA spectra of hexagonal ice (Ih) and liquid water and interpreted the significantly different profiles in terms of an important amount of undercoordinated molecule and strongly distorted or broken H bonds in the liquid sample. They observe that some characteristic spectral features associated with the redistribution of charge through the tetrahedral H-bond network of ice Ih are significantly weakened in the spectrum of liquid water. On the other hand, the latter shows some similarities with the spectrum obtained from the surface of ice, where the percentage of acceptor only molecules is known to be large.[7]

The traditional picture of symmetric first coordination shells in liquid water, with more than 80% of the molecules forming two donating and two accepting H bonds, has been widely supported by molecular dynamics (MD) simulations by using established empirical potentials. The radial distribution functions (RDFs) generated by symmetric models with fleetingly broken H bonds, in general, fit rather well to x-ray and neutron diffraction data. However, it has been shown recently that an analogous agreement with all the diffraction data can be obtained with very different structures, including samples characterized by strongly distorted H-bond networks.[8] These results open new possible interpretations of the experimental data, since a very large variety of structural solutions seem to provide similar fit quality, irrespective of local coordination and H-bond statistics. It has been also reported that taking into account quantum effects through path-integral simulations based on empirical force fields results in a less structured liquid that shows better agreement with experiment for several thermodynamic and dynamical properties.[9,10]

On the other hand, *ab initio* models displaying large percentage of double donor (DD) and double acceptor (DA) O atoms often fail in reproducing measurable properties, such as diffusivity or even O–O RDF. Among other factors that may be responsible for these discrepancies, it has been pointed out that the available exchange and correlation (XC) functionals are often not adequate to describe such a com-

[a)]Electronic mail: marcella.iannuzzi-mauri@psi.ch.

plex dynamic system governed by fluctuating H-bond networks.[11–15] Other sources of inaccuracy have been identified in the limited size of simulation cells and in too short equilibration times of typical *ab initio* MD runs. These conditions are likely to prevent a proper statistical sampling of the thermodynamic equilibrium. Therefore, even the *ab initio* MD simulations performed until to now seem not to be sufficiently reliable to give a conclusive answer about the structure of liquid water.

Different theoretical approaches for core level spectroscopy calculations based on density functional theory (DFT) and the Kohn and Sham (KS) formalism,[16] have been proposed to investigate the spectrum of liquid water.[2,17–21] It is indeed necessary to identify clearer relationships between specific features of the spectra and the corresponding H-bond connectivity. Such knowledge can then be used in the interpretation of experimental results. Standard full potential calculations employ Gaussian-type orbitals (GTOs) as basis set functions, associated with cluster model approximations to represent extended systems. Very large basis sets on the excited atom, including many extended functions, are often required to guarantee the necessary flexibility in the description of the unoccupied states involved in the core-hole creation process. On the other hand, plane wave (PW) basis sets accompanied by the pseudopotentials are typically employed in combination with the supercell approach. In this case, the core level orbitals are not directly available. They are treated as frozen, without taking into account any relaxation effect, while the core state energies are approximated by the corresponding atomic values. Moreover, in the core region, the valence wavefunctions are approximated by pseudowavefunctions. The transition oscillator strengths can be either approximated through the pseudowavefunctions, or they can be reconstructed *a posteriori*, e.g., applying the projector-augmented-wave technique.[22]

The x-ray absorption spectra of ice Ih and liquid water presented in this work are obtained by applying a newly implemented scheme for inner-shell spectroscopy simulations in condensed matter, which is based on the Gaussian augmented plane wave (GAPW) formalism,[23,24] and is available in the CP2K program package.[25] The GAPW method relies on GTO to expand the molecular orbitals (MOs), while PW representations are used only for the soft part of the charge density. Thanks to this hybrid basis set scheme, the calculation of the time consuming, two electron Coulomb integrals can be avoided leading to a linear scaling construction of the Hamiltonian. The method is suitable for all-electron calculations on several hundreds of atoms. For condensed matter calculations, it can be used in combination with the supercell approach and the periodic boundary conditions (PBCs). The spectral distributions are obtained from the solution of the KS equations computed with a modified core density at the absorbing atom, such that the relevant relaxation effects induced by the core hole are fully taken into account. By this approach, neither pseudopotentials nor frozen cores are imposed, and finite size effects can be avoided by turning on the PBC. The oscillator strengths are computed through dipole integrals between the core orbital and the available valence and unoccupied states.[26] More details about GAPW inner-shell spectroscopy simulations are given by Iannuzzi and Hutter.[5] In the same paper, the method has been validated through a set of XAS simulations on simple molecules in gas phase. The choice of basis set and core all potential has also been extensively discussed.

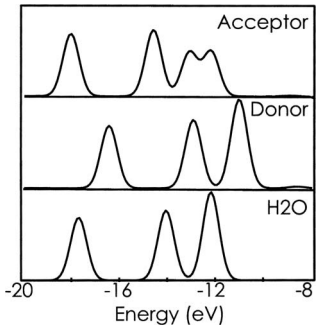

FIG. 1. Computed O 1*s* emission spectra of isolated water molecule (bottom), dimer's donating molecule (middle), and dimer's accepting molecule (top). On the abscissa, the binding energy, $E_b=\varepsilon_f-\varepsilon_{1s}-IP_{1s}$, is reported.

In order to mimic the experimental line broadening, the theoretical spectra reported in this work are Gaussian convolutions of the discrete oscillator strengths. Below the ionization threshold, the Gaussian functions have fixed width of 0.5 eV, while linearly increasing width, up to 8 eV, is used over the following 20 eV. The spectral lines are averaged over the three Cartesian directions and the resulting curve is normalized within the displayed energy interval. The on-set energy of the absorption spectrum is always aligned with the ΔSCF O 1*s* first excitation energy, as obtained in separated calculations carried out for each considered sample and using the same simulation setup (basis set, XC functional, box).

II. WATER DIMER

The formation of hydrogen bonded networks is responsible for profound changes in the properties of liquid water and ice with respect to the gas phase. The interaction between two H_2O molecules induces the rehybridization of the antibonding orbital along the donating O–H bond, thus, minimizing the repulsion between the electronic clouds. This is accompanied by a partial charge redistribution between the acceptor and the donor O atoms. The rearrangement of the electronic structure is already relevant going from the isolated water molecule to the water dimer. The changes in the charge density distribution are associated with well identified variations in the spectral profile, as shown by the O 1*s* x-ray emission spectra (XES) reported in Fig. 1 as well as by the XA spectra reported in our preceding work.[5] The emission spectra are obtained from energy differences and oscillator strengths computed between the occupied ground state orbitals, following the formalism suggested by Triguero *et al.*[26] The absorption spectra, instead, are obtained by employing the half-core-hole (HCH) formalism. For all the calculations, Becke–Lee–Yang–Parr (BLYP) XC functional[27,28] and aug-cc-pV5Z basis set[29] are used. High quality basis sets are needed to capture the fine structure of the unoccupied orbitals. The resulting emission and absorption spectra for the isolated molecule agree well with the results reported by

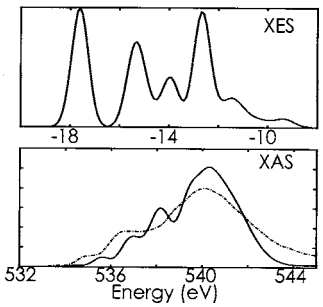

FIG. 2. O 1*s* emission spectrum (top panel) and HCH absorption spectrum (bottom panel) computed for the 64 molecule box of Ice Ih by applying the 6-311G(*d*,*p*) basis set. Dot-dashed line: experimental absorption spectrum taken from Ref. 33 for direct comparison.

Nilsson *et al.*[33] The XES profile of the donor O displays the same three characteristic valence bands as the spectrum of the isolated molecule, but shifted toward lower binding energies. The shift is determined by the partial charge transfer from the acceptor's lone pair to the donor, upon formation of the H bond. The third band in the acceptor's XES curve is instead split into two peaks of reduced intensity. In the isolated molecule, this band corresponds to the occupied lone pair orbitals. By dimerization, these states are partially emptied. The H-bond signature is even more evident from the absorption spectra, which describe the local character of the unoccupied MOs. The emptied lone pair orbitals on the acceptor are responsible for increased intensities above 542 eV. The split of the first resonance and a general weakening of the pre-edge features characterize, instead, the donor's spectrum. These changes in the low part of the spectrum, are counterbalanced by broader and larger structures at higher energy, which are associated with orbitals distributed among the two O atoms.

III. ICE IH

In hexagonal ice each molecule is at the center of a tetrahedron formed by its four first neighboring molecules, and each O atom participates in four H bonds, being simultaneously two times donor (DD) and two times acceptor (DA). The emission and the absorption spectra reported in Fig. 2 are generated from the optimized geometry of a supercell containing 64 H_2O units (box axis $a=8.9845$ Å, $b=15.5612$ Å, $c=14.6718$ Å). The GAPW calculations are performed with 6-311G(*d*,*p*) basis sets,[29–32] the BLYP functional, and a PW cutoff of 250 Ry. Such setup provides 1920 orbital functions (OFs) to expand the MOs. The x-ray absorption spectrum has been generated by the HCH potential. The main features characterizing the experimental spectra reported by Nilsson *et al.*[33] are correctly reproduced by the simulation. In analogy with what observed for the dimer, the XES splitting of the central $3a1$ band is due to the rehybridization of the valence orbitals. The rehybridization minimizes the repulsive interactions among the overlapping electronic clouds and stabilizes the hydrogen bonding. The XAS in Fig. 2 is rigidly shifted by −2.16 eV, in order to align the first excitation energy to the value obtained by ΔSCF, and the convolution is normalized in the displayed energy interval. Within the same interval, about 200 unoccupied final states are available per each absorbing O center. In fact, the spectral distribution is obtained from the convolution of about 40 non-negligible oscillator strengths.

The pre-edge structure, at about 534 eV, associated with the unoccupied O–H antibonding orbitals and observed in gas phase, disappears for the pristine, tetrahedral lattice. Another distinguishing feature of ice's XAS is the dominant postedge band, centered around 540 eV, which collects the contributions from the emptied lone pair orbitals. The main-edge oscillator strengths form a step-shaped shoulder between 536 and 538 eV. Also, these features can be attributed to the orbital rehybridization and charge redistribution occurring upon condensation, as already discussed by Cavalleri *et al.*[34] The computed absorption spectrum reproduces the main experimental features discussed above. However, we observe that our model produces narrower and more pronounced bands, most probably due to the contraction in the energy distribution determined by the localization of more states in small energy intervals. This causes the appearance of an additional peak at 538 eV, and a general intensity reduction of the stepwise shoulder located at lower energies. The resulting profile looks to be overstructured, showing two peaks separated by a pseudogap around 538.5 eV.

A. Basis set and supercell size

By core level spectroscopy, we address the projection of the MOs onto the ionized core. In order to properly describe the relevant unoccupied orbitals, i.e., those with significant overlap with the excited core orbital, it is important to have an adequate representation of the MOs in the region around the absorbing atom. In this respect, improvements are possible by selecting basis sets of better quality, i.e., with more OFs and increased flexibility. In this work, four simulation cells of different size, from 16 to 432 molecules, have been considered, and for each of them different basis sets. The selected basis set combinations are 6-311G(*d*,*p*) (B1); aug-cc-pVQZ on the absorbing O center and 6-311G(*d*,*p*) on all the other atoms (B2); cc-pVQZ (B3); IGLO-III (B4); IGLO-III on *H* and aug-cc-pVQZ on O (B5); cc-pVQZ on H and aug-cc-pVQZ on O (B6); cc-pV5Z (B7). Table I summarizes for each of the tested supercell/basis sets combination choice the total number of OFs, the number of low-energy unoccupied states (LUSs), i.e., with excitation energies up to 543 eV, and the number of LUS that significantly contribute to the spectrum, i.e., with non-negligible transition probability (TPS). These latter are those states that significantly overlap in space with the localized core orbital and that are accessible, according to the selection rules. Although the number of OFs and LUS can become rapidly large by changing basis set and by increasing the supercell size, the variations in the number of TPS are much smaller. This happens because functions centered far from the the absorbing atom contribute very little or not at all to the spectrum.

Figure 3 shows the variations of the HCH XAS profile with the basis set for the two smallest simulation cells, containing 16 molecules (top panels) and 64 molecules (bottom panels), respectively. For the 16 H_2O box, the overstructuring of the spectrum is pronounced, in particular, when poor

TABLE I. For different box sizes, going from 16 to 432 water molecules, total number of available OFs, number of available unoccupied states up to 543 eV LUS, and number of non-negligible oscillator strengths in the same energy interval TPS.

	16 molecules			64 molecules			128 molecules			432 molecules		
Basis	OF	LUS	TPS	OF	LUS	TPS	OF	LUS	TPS	OF	LUS	TPS
B1	480	32	23	1920	94	61	3840	186	85	12960	593	89
B2	542	42	30	1982	126	69	3902	244	87	13022	707	100
B3	1840	50	37	7360	174	76						
B4	880	50	34	3520	189	83	7040	367	101			
B5	1600	51	39	6400	202	84						
B6	2203	52	39	7560	181	85						
B7	3216	49	40									

basis sets are used. By improving the quality of the basis set, the fore peak of the main body of the spectrum (~538.5 eV) is smoothed out and the overall shape resembles more closely the experimental curve. Better agreement with experiment is obtained with the 64 molecule box. The largest divergences are observed in the lowest part of the spectrum. Also, in this case, the initial spectrum is overstructured, but becomes progressively smoother with larger basis sets, thus approaching the steplike shape of the experimental curve. In both cases, the spectrum converges to its final shape already with B4. The main differences between the converged distributions and the experimental results are too compact postedge bands, with maximum shifted downward and higher intensities, and the presence of the second peak between 536 and 538 eV, even if less pronounced for 64 H_2O.

The spectral distributions obtained with larger samples, containing 128 and 432 molecules, turn out to be already converged with the B2 basis set, as shown in Fig. 4. In this case, no additional peak appears below 538 eV. The curves are smooth and follow the expected steplike behavior. The main body of the spectrum closely reproduces the correct distribution of the postedge oscillator strengths.

The fact that in all the discussed cases, the distribution turns out to be more compact and the postedge band too intense with respect to experiment can be justified taking into account that our calculations are performed on pristine ice samples, where all the oxygen atoms are equivalent. The experiments, instead, are performed on samples containing a certain degree of disorder. As discussed by Nordlund *et al.*,[7] the postedge width is sensitive to the disorder in the sample and there is a substantial broadening and lowering of the apparent height in more surface sensitive spectra due to the presence of an amorphous region close to the surface. Moreover, additional broadening of the postedge band has been attributed to the very short lifetime measured by Auger spectroscopy for the electrons excited to the corresponding energies.[35] These broadening effects are not included in the theoretical model used in the present work.

From the discussed results, we infer that certain type of overstructuring at lower energy is most probably due to the limited size of the sample and to the consequent artificial confinement of the wavefunctions. Too small supercells hamper the correct description of the electronic structure of an extended system. In hydrogen bonded systems, this behavior is enhanced by the long range connectivity and by many-body effects. Therefore, the optimization of the charge density in presence of a core hole is going to be affected by the confinement of the wavefunctions imposed by too small su-

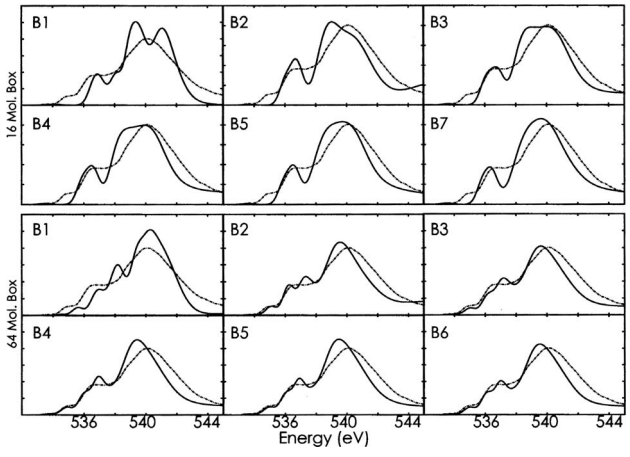

FIG. 3. XA spectra computed for the 16 molecule cell and the 64 molecule cell with basis sets of different quality. More details about the selected basis sets are given in the text and in Table I. The experimental curve from Ref. 33 is reported in each panel for direct comparison (dashed line).

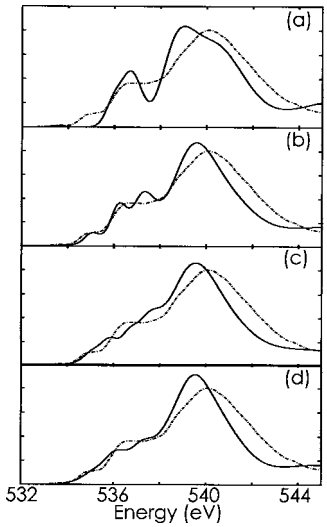

FIG. 4. Ice O 1*s* XA spectra computed for simulation boxes containing (a) 16, (b) 64, (c) 128, and (d) 432 H_2O molecules using the basis set B2 of Table I. The dot-dashed line is the experimental curve from Ref. 33.

percells or cluster models. Moreover, too small simulation cells under PBC might also introduce artifacts due to unwanted interactions between the core-hole images. Within this picture, the strongly overstructured spectrum obtained with 16 H_2O can be interpreted as an effect of the excessive localization of the LUSs, as induced either by the enforced periodicity or by the high concentration of core-hole images, placed at less than 8 Å. In order to avoid misinterpretations of the computed spectra is, therefore, essential to represent correctly the extended character of the wavefunctions.

B. Quantum mechanics/molecular mechanics XAS simulations

Further investigations on the role of the correct representation of the extended character of the wavefunctions is carried out by exploiting the hybrid quantum mechanics (QM) molecular mechanics (MM) approach, as implemented in CP2K,[25,36] Standard PBC are applied to the MM box, while the internal QM part is correctly replicated inside each image of the supercell, by applying the electrostatic coupling/decoupling approach introduced by Blöchl.[37] We adapted the original periodic QM/MM scheme to allow its use together with the GAPW formalism.

Starting from the box containing 432 molecules, the QM region is defined by centering it on the absorbing oxygen. The same DFT setup described above is employed for the QM section, whereas the rest of the system is treated at the TIP3P force field level.[38] In order to verify how the local orbital structure and the rearrangements induced by the creation of the core hole are susceptible to the perturbation of the wavefunctions at large distance, the QM subsystem is increased progressively. The smallest subsystem contains only the first coordination shell around the absorbing molecule, i.e., five molecules in total. The other three subsystems contain 17, 42, and 83 water molecules, which are always symmetrically distributed in a spherical region around the first absorbing one. The largest subsystem corresponds to a radius of about 8 Å. By selecting basis sets of different qualities, we also take into account the possibility of compensating the finite size effects by using more polarization functions and diffuse functions.

Figure 5 shows the spectra computed for the QM/MM systems containing 5 and 17 QM molecules, left and right panels, respectively. Four basis sets have been selected, 6-311(d,p) (B1), IGLO-III (B2), cc-pVQZ (B3), and aug-cc-pVQZ (B4). When only the first coordination shell is included in the QM subsystem, strongly structured spectra are generated, which are rather different from the reference full QM spectrum (thin solid line). No clear improvement is achieved by changing the basis set. With 17 molecules in the QM region, the spectra are characterized by a small peak in the pre-edge region, depletion in intensities above 536 eV, followed by a pronounced main-edge structure. Main-edge and postedge oscillator strengths form two almost equivalent bands that merge in the middle, at about 539 eV, giving rise to a two-peaked curve with a pseudogap in between. As a consequence, the postedge band is pushed upward with respect to the full QM spectrum. Also, when B4 is applied, the

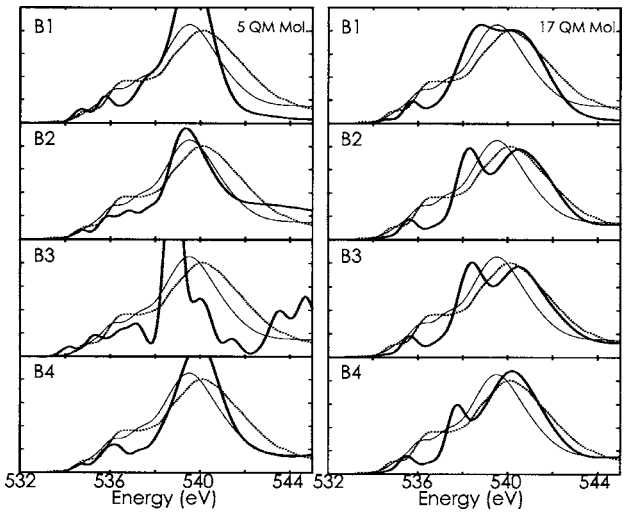

FIG. 5. QM/MM O 1s XAS computed for the supercell containing five QM molecules (left panels) and the supercell containing 17 QM molecules (right panels) with different basis sets, as described in the text. The full QM spectrum (thin line) and the spectrum obtained from experiment (dashed line) are also reported for comparison.

two peaks persist, even if the lowest in energy becomes less intense and moves downward. By increasing the QM subsystem, the XAS profile tends slowly toward the full QM spectrum, as shown in Fig. 6, where the spectra computed for boxes containing 42 and 83 water molecules are displayed. The pre-edge structure gets smoother, the main-edge band is shifted downward and fills the depletion region above 536 eV, the characteristic shape of the postedge band is recovered. However, the lowest energy part of the spectrum is still overstructured, even with the largest QM subsystem and the largest basis set that could be used for this simulation cell. The truncation of the electronic structure at the border of the QM fraction induces distortions of the MOs, which affect the spectral distribution. As occurred when too small supercell were considered, the typical effects of the confinement are the enforced localization of the wavefunctions and the more structured spectrum, characterized by well distinguished band.

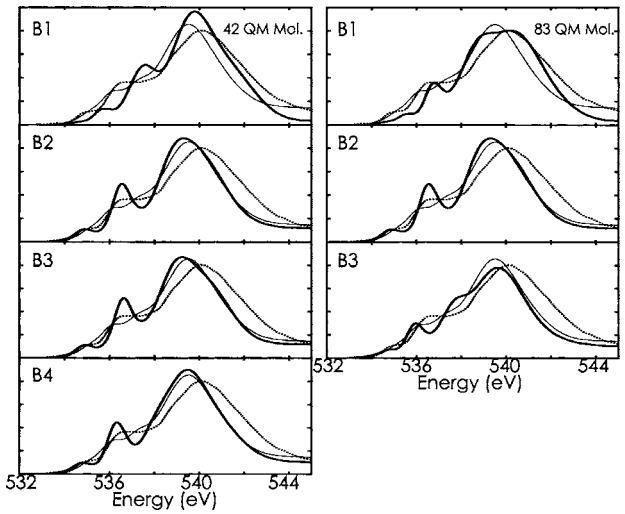

FIG. 6. Same as Fig. 5 for the supercell containing 42 QM molecules (left panels) and the supercell containing 83 QM molecules (right panels).

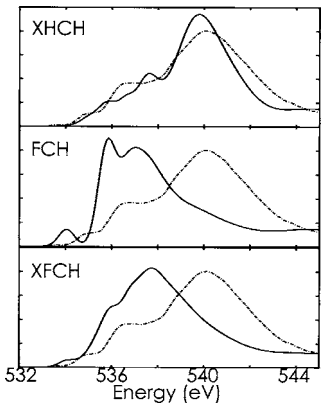

FIG. 7. XHCH, FCH, and XFCH spectra computed for the 128 molecule ice sample with the B2 basis set of Table I. The experimental curve from Ref. 33 is always reported as reference (dashed line).

The results discussed in the previous paragraphs indicate once more that it is essential to take into account the extended character of the electronic interactions, even if we look at local processes such as core state excitations. This is especially true for systems such as water, where the molecular connectivity is enhanced by the network of H bonds. Similar conclusions led Prendergast and Galli[20] to advocate *k*-point sampling, as necessary to optimally reproduce the experimental XAS of bulk ice starting from a supercell of 64 molecules.

C. Core-hole potential

Another aspect related to XAS calculations that needs to be considered is the choice of the core-hole potential. This problem has been discussed in recent publications, where the half-core-hole and the full-core-hole (FCH) spectra of ice and liquid water have been compared.[18–20] In our previous paper,[5] four forms of the core-hole potential have been tested on small molecules in gas phase. Beside the most common HCH and FCH potentials, the excited-half-core-hole (XHCH) and the excited-full-core-hole (XFCH) have also been considered, by locating the removed half or full core electron into the first unoccupied state. The results discussed in that work confirm that the FCH potential amplifies the oscillator strengths related to the first unoccupied orbitals, because of its strongly attractive character. XHCH and XFCH, instead, induce downwards shifts of the second half of the spectrum, thus reducing the separation between pre-edge and main-edge. The HCH potential, in contrast, has the tendency of enhancing the postedge part of the spectrum. For the studied cases, it has been observed that, even if the main features of the computed spectral profiles are correctly reproduced by all the four representations, the best description of the fine structure is achieved by HCH.

A similar comparison is proposed in this work for the spectrum of ice. Figure 7 shows the spectra obtained for the simulation cell containing 128 molecules with the B2 basis set of Table I. All of the spectra are aligned to the first ΔSCF excitation energy, as obtained with the same setup. This means that the half-core spectra are shifted downward of about 2 eV and the full core spectra of about 14 eV, since the completely emptied core state falls much deeper in energy. The XHCH spectrum, top panel of Fig. 7, resembles closely the HCH spectrum reported in Fig. 4, thus reproducing the main features of the experimental curve. The FCH, instead, leads to an overall displacement of the distribution toward lower energies. Some states at about 534 eV acquire notable intensities, while the oscillator strengths at higher energies are distributed over a more compact interval, resulting in a spectrum with a two-peaked main body. In place of the broad steplike shoulder, the main-edge oscillator strengths form a narrow band, with maximum at 536.5 eV. The shifted postedge intensities form a band which is merged with the previous one and decays rapidly above 538 eV. This behavior can be explained in terms of the strongly attractive FCH potential, which induces the contraction of valence and of first unoccupied orbitals, with the resulting enhancement spectral intensities below 538 eV. On the other hand, the outer unoccupied states turn out to be more delocalized, due to the screening of the compact lower bands, and therefore their overlap with the ionized core is reduced. These effects are attenuated by placing the excited electron in the lower unoccupied orbital, i.e., using the XFCH representation, and indeed, there are some improvements in the spectral profile with respect to the FCH results. The broad and dominant postedge band and a steplike structure formed by the main-edge oscillator strengths can be distinguished, and there are no notable pre-edge structures. Nevertheless, the contraction of the bands and the downward shift of the second half of the spectrum are still present. In conclusion, HCH and XHCH are confirmed to provide the best agreement with experiment, in particular, with respect to the energy distribution of the oscillator strengths. The FCH model potential turns out not to be adequate to reproduce the rearrangements of the electronic structure induced by the absorption process, while the XFCH partially restores the balance between initial and final states of the transition.

IV. LIQUID WATER

The commonly accepted model of liquid water, where each O is, most of the time, involved in the formation of four stable H bonds, being simultaneously a double donor and a double acceptor, has been recently questioned.[6] A picture of a less coordinated structure, with large percentage of broken or very weak H bonds, has been proposed on the basis of the interpretation of x-ray absorption spectra, as compared to the spectra of bulk ice and of the surface of ice. If correct, this interpretation would also be in conflict with most of the theoretical models of the liquid, which also assume symmetrically, fourfold coordinated molecules. A variety of classical and *ab initio* MD simulations of liquid water have been carried out in the past years and have shown large discrepancies in either structural or dynamical properties. Recently, it has been demonstrated that several technical factors, among which the choice of the XC functional, are at the origin of the disagreement of *ab initio* results with experiment and among themselves.[14,15,39]

In the present work, we do not want to address the reliability of *ab initio* MD simulations of liquid water. Our aim

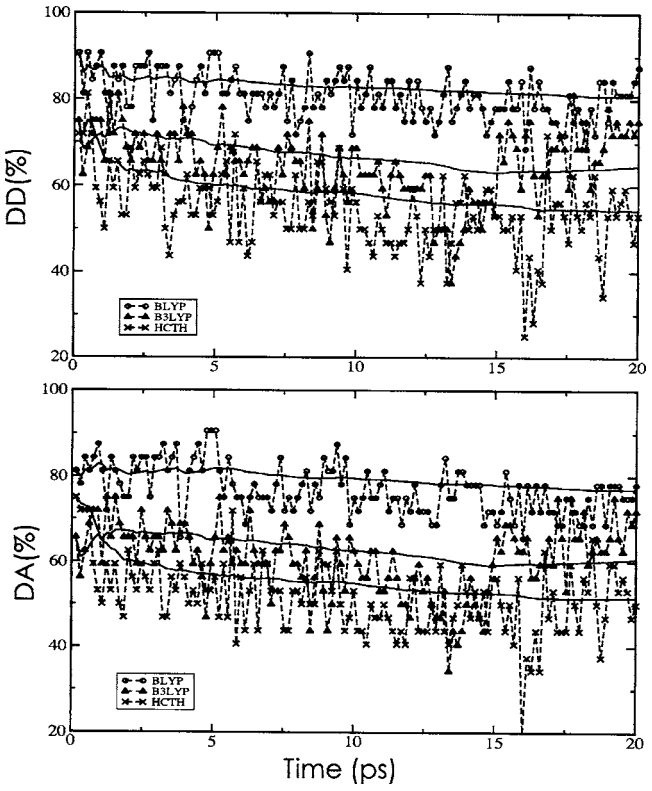

FIG. 8. Percentage of DD (a) and DA (b) oxygen atoms along the three *ab initio* MD trajectories generated with BLYP, B3LYP, and HCTH407 XC functional, respectively. The mean values are indicated by the thick lines.

is to understand the links between computed x-ray absorption spectra and the corresponding structural properties of the liquid sample in use. For this purpose, we have carried out XAS calculations on snapshots extracted from three different MD trajectories, which have been generated with three different XC functionals, BLYP, B3LYP,[40] and HCTH407.[41,42] The simulation cell contains 32 water molecules and for all the MD calculations, Goedecker type of pseudopotentials[43] have been used. The BLYP and the HCTH407 trajectories are taken from those analyzed by VandeVondele *et al.*[15] in their work on the influence of temperature on RDF. The B3LYP trajectory, instead, has been provided by Teodorova *et al.*,[44] who tested different hybrid density functionals.

The RDF and the diffusion coefficient computed from these three trajectories indicate that BLYP generates the most structured sample, followed by B3LYP. The HCTH407 trajectory shows more diffusive and liquidlike behavior. This means that, by selecting different XC functionals, it is possible to tune the rigidity of the first coordination shell around the water molecule, thus having more fleeting hydrogen bonding. Namely, less structured samples are expected to be characterized, in average, by a smaller number of strong H bonds and more asymmetrically coordinated oxygens.

Figure 8 displays the fluctuations in the number of DD and DA oxygen atoms along the three selected trajectories. We adopt the definition of H bond proposed by Wernet *et al.*,[6] where the maximum O–O distance depends on the distortion of the bond. The conventional maximum distance of 3.3 Å is used for linear H bonds. This is linearly decreased to

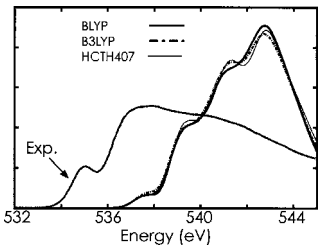

FIG. 9. HCH XA spectra generated from MD samplings. Each curve is the average over the spectra of 40 snapshots taken along the BLYP trajectory (solid line), the B3LYP trajectory (dot-dashed line), and the HCTH407 trajectory (thin-solid line). The dotted line is the experimental curve as reported in Ref. 6.

a minimum of 2.6 Å for bent bonds, with maximum accepted bending of 45°. The mean values reported in Fig. 8 show that the percentage of DD and DA decreases from above 80% for BLYP, to below 60% for HCTH407, where a few snapshots reach low points of 30% DD and 35% DA. The fluctuations in the instantaneous values are still large after 20 ps of simulation time, and the averages seem not to have reached their equilibrium value at the end of the provided runs. However, the well separated mean values confirm that the average coordination in the three samples is not equivalent, in agreement with the trend indicated by the RDF. Such structural fluctuations should induce rearrangements of the electronic structure that can be resolved by the x-ray absorption technique.

In what follows, we discuss trajectory spectra, single-snapshot spectra, and individual-oxygen spectra. The single-snapshot spectra are obtained as averages over the K edges of all the 32 oxygens contained in the simulation cell, at a given MD iteration. The spectrum representing one entire trajectory is obtained as the sum of 40 single-snapshot spectra computed for evenly distributed snapshots, one every 0.5 ps. All of the spectra calculations are performed with BLYP functional and all-electron basis sets on all the atomic centers. The computed XA spectra are always aligned with the first ΔSCF excitation energy obtained with the same setup (i.e., same simulation cell, functional, and basis sets) and normalized in the displayed energy interval.

First, we compare the three trajectory spectra obtained with HCH potential and 6-31G(d,p) basis sets, corresponding to 768 OF for the entire box. When the 6-31G(d,p) is used, the ΔSCF on-set value is about 537 eV, i.e., 3 eV higher than the experimental value. The three spectra are shown in Fig. 9 together with the experimental curve (dotted line), as borrowed from Wernet *et al.*[6] The experimental spectrum of liquid water is characterized by an overall downward shift of the center of the distribution, with respect to the spectrum of bulk hexagonal ice. Some pre-edge states gain in intensity forming a first peak at about 537 eV. The main-edge band becomes dominant, whereas the smoothed post-edge tail is distributed over a larger energy range, resulting in a general intensity reduction. These deviations from the ice XAS have been interpreted in terms of an increasing number of broken H bonds. Within this picture, we should expect a reduced incidence of rehybridization of antibonding O–H

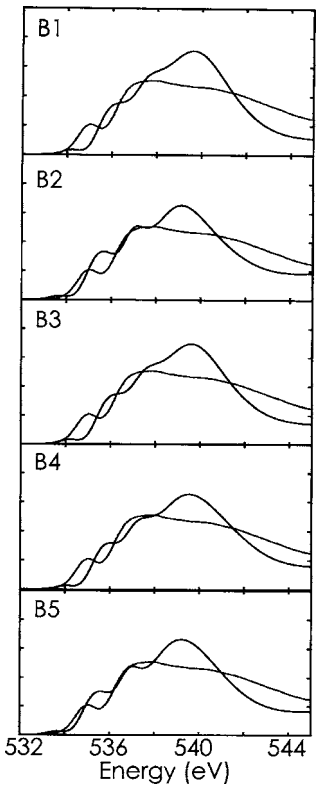

FIG. 10. HCH XA spectra computed with different basis sets on one snapshot extracted from the HCTC407 trajectory. The description of the basis set B1–B5 is given in the text. The dotted line is the experimental curve, as reported in Ref. 6.

and lone pair orbitals associated with the attenuation of the characteristic signature of symmetrically coordinated O in the spectral distribution.

All of the 6-31G(d,p) spectra in Fig. 9 are shifted to too high energy, and have compact and intense bands. We notice only a slight decrease in the postedge intensities, together with a small increment in the main-edge region. Moreover, there are only very small differences going from the BLYP trajectory to the least structured sampling generated by HCTH407. The first peak, which should denote the presence of broken H bonds, is replaced by a smooth shoulder at about 539 eV. This feature becomes only slightly more pronounced in the HCTH407 spectrum. Although the spectral profile shows the tendency to evolve in the right direction, the differences are by far less pronounced than what expected, and the three spectra turn out to be rather similar to the spectrum of ice, at least with this simulation setup.

A. Basis set

One possible source of inaccuracy is the use of a basis set of insufficient quality. These calculations are computationally intensive, because a large number of oscillator strengths needs to be computed for each O atom and each configuration taken into account. Therefore, in order to address the influence of the basis set, we focus on one single snapshot taken from the HCTC407 trajectory. The selected snapshot is characterized by having 90% of DD oxygens, 84% DA, and 78% forming DD-DA configurations. XAS simulations are performed with five different basis sets. The combinations of basis sets that have been considered are 6-311G(d,p) (B1) providing 960 OF, aug-cc-pVQZ on the absorbing oxygen and 6-311G(d,p) otherwise (B2) providing 1022 OF, 6-311G(3df,3dp) on all O and 6-311G(d,p) on H atoms (B3) providing 1504 OF, 6-311G(3df,3dp) on all the atomic centers (B4) providing 2208 OF, aug-cc-pVQZ on all O and 6-311G(d,p) on H atoms (B5) providing 2944 OF. The alignment to the first ΔSCF excitation energy gives good agreement with experiment already with B1. The five profiles displayed in Fig. 10 are rather similar. All of them show a compact and peaked postedge band, suggesting a predominance of symmetrically coordinated oxygens. However, with respect to ice, we notice a general decrease in the intensities beyond the edge, in favor of the lower energy part of the spectrum. The clearly predominant postedge structure denotes that in the selected snapshot, the majority of the oxygen atoms are DD-DA, with symmetric coordination shell. Nevertheless, an excessive amplification of this effect is also possible due too to the limited size of the sample. It is interesting to notice that, when B2 and B5 are employed, i.e., by including some augmented functions on the absorbing oxygen, the shape of the pre-edge and main-edge structures follows more closely the experimental curve.

B. XAS of single snapshots

In order to better identify the signature of broken H bonds and asymmetric coordination shells, spectral contributions of specific configurations are considered separately. The role of asymmetrically coordinated oxygens is revealed by comparing the spectra obtained from snapshots with different amounts of DD and DA centers. Six snapshots have been selected from the HCTH407 trajectory, containing from 78% to 22% DD-DA molecules. The XA spectra displayed in Fig. 11 are calculated with B2 and the HCH potential. The

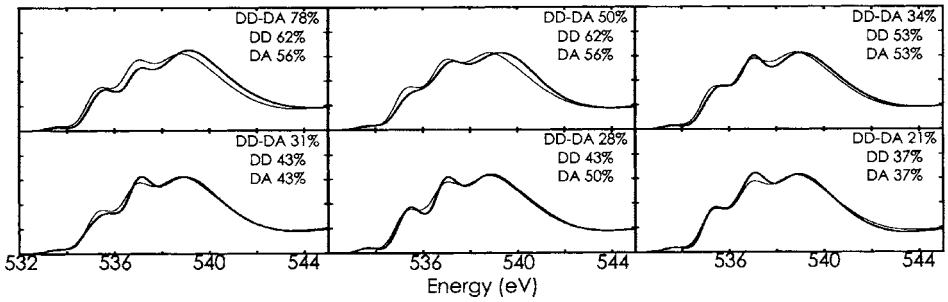

FIG. 11. HCH XA spectra computed with B2 on six MD snapshots extracted from the HCTH407 trajectory. The percentage of DD-DA configurations is indicated per each snapshot. Thin line: spectrum averaged over the selected 40 snapshots from the same trajectory and using the same potential.

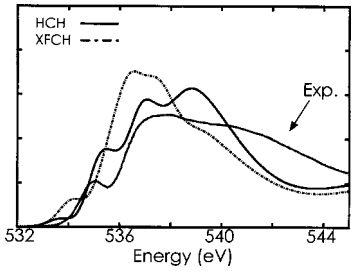

FIG. 12. HCH (solid line) and XFCH (dot dashed) XA spectrum averaged over the selected 40 snapshots extracted from the HCTH407 trajectory.

percentage of DD-DA configurations as well as the percentage of oxygens that are at least DD or at least DA are indicated in each panel of the figure. The trajectory spectrum generated from the HCTC407 sampling is reported as reference (thin line). By decreasing the number of DD and DA oxygens, a progressive depletion of the postedge band is observed, while the structures located at lower energy become more pronounced. Although the postedge is still dominant when DD-DA represent 78% of all the oxygens, this effect lessens for structures containing a larger number of broken H bonds. In particular, the relative height of the main-edge maximum (~537 eV) and postedge maximum (~539 eV) evolves with the number of DA, while variations in the number of DD affect primarily the first peak, below 536 eV. We notice a clear trend of the XAS profile toward the experimental curve while the H-bond network becomes looser. However, the maximum of the postedge band, at about 539 eV, persists, most likely due to the excessive localization in energy of the postedge oscillator strengths. Hence, the broad-longtailed shape observed by experiment is not fully reproduced by the calculation. If the interpretation given by Wernet *et al.*[6] is correct, these results indicate that, in our MD sampling, the rehybridization due to the interaction of the molecule with its first shell of neighbors is still predominant. This seems to be the case even for many of those molecules with strongly distorted and asymmetric coordination shells, i.e., identified as SA and/or SD.

C. XFCH core-hole potential

It has been already remarked that the HCH potential has the tendency to amplify the intensities in the postedge region. However, as discussed in our previous paper[5] and in this work for the case of ice Ih, the full core-hole potential might have the opposite effect of boosting the oscillator strengths in the lower part of the spectrum. The XFCH spectrum calculated for ice, instead, shows better agreement with experiment than FCH, even if the downward shift of the postedge oscillator strengths is still large (~2.5 eV), resulting in a rather compact distribution. This behavior is confirmed by the XFCH spectrum computed over the HCTH407 trajectory and showed in Fig. 12. This spectrum has been obtained with the B2 basis set of Fig. 10 and it has been rigidly shifted 13 eV downward, in order to align the on-set energy to the ΔSCF first excitation energy. For a consistent comparison, the shifted spectrum has been normalized in the displayed energy interval. The variations with respect to the XFCH spectrum of ice (see Fig. 7) are attributed to the presence of undercoordinated water molecules and asymmetric hydrogen bonding, as already discussed for the HCH case. We recognize some common features as the enhancement of main-edge with respect to a the less intense postedge band, and the appearance of a first small pre-edge structure, at 534 eV for XFCH. The XFCH characteristic contraction together with the shift of the postedge band generate one compact structure centered around 537 eV, while at higher energies, the intensities drop rapidly. In summary, both the HCH and XFCH spectra display characteristic features that denote the presence of asymmetric coordination shells in the liquid sample. However, the HCH energy distributions are in better agreement with the experimental findings and also the relative intensities, as, for example, between the first peak and the main body of the spectrum, are better reproduced by using the half-core scheme.

As for HCH, the behavior of XFCH spectra triggered by variations in the amount of asymmetrically coordinated oxygens has been investigated. A similar trend, as observed with HCH, is revealed from the comparison of the six spectra generated from snapshots with different contents of DD-DA molecules (see Fig. 13). At lower percentage of DD-DA, the main front structure is amplified, whereas the region between 539 and 540 is slightly depleted. The pre-edge structure, instead, seems not to be significantly affected, in contrast with HCH.

D. XAS of individual O

We have shown that irrespective of the core-hole potential, the method is sensitive to the average coordination of the water molecules and to the presence of weak and broken H bonds. A further proof of this behavior is presented in Fig. 14, where the *K* edges of single O atoms taken from the liquid sample are compared to the spectrum sampled over the trajectory. From this figure, it emerges clearly that changes in the coordination shell of the oxygen affect strongly the spectrum profile. The spectra of DD oxygens (first and second

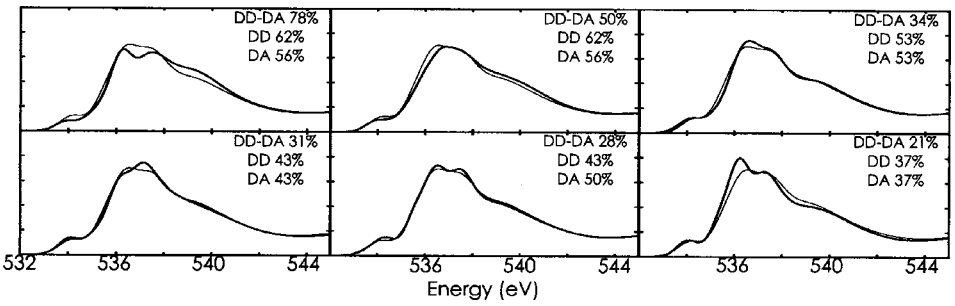

FIG. 13. XFCH XA spectra computed with B2 on six MD snapshots extracted from the HCTH407 trajectory. See caption of Fig. 11.

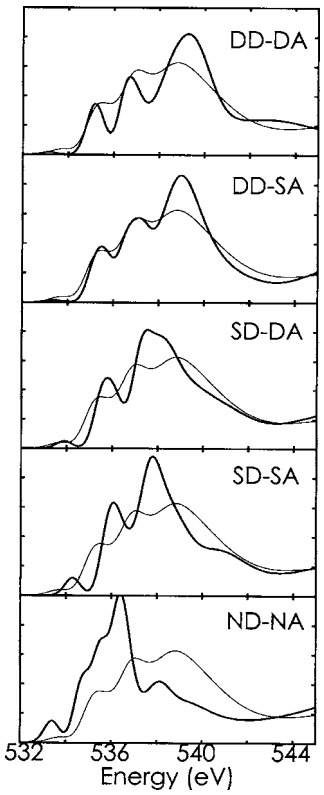

FIG. 14. *K* edges of single O atoms with different coordination shells taken from one snapshot of the HCTH407 trajectory. The spectra are computed with the HCH potential and B2 basis set. The dot-dashed line is the spectrum averaged over the sampling.

panels) show dominant postedge bands centered about 539 eV and two distinct bands at lower energy. The overall shape recalls the profile of the spectrum of hexagonal ice, even if significant differences remain also for the DD-DA. Namely, the liquidlike environment affects the rehybridization of the orbitals overlapping with the absorbing core state, preventing the complete charge redistribution through the H bonds, as described for the ice electronic structure.[33] The SD configurations give rise to spectra which are closer to the experimental XAS of water, having a fore peak at 536 eV, followed by a broader band with maximum in the main-edge region. The postedge is progressively depleted, the center of the distribution moves downward, while the intensities below the edge increase. When no H bond (ND-NA) is formed, the rehybridization does not take place, the lone pair orbitals are occupied, and the postedge band is quenched.

These last results confirm that changes in the shape and relative intensities of pre-edge, main-edge, and postedge can be identified as signatures of the presence of different H-bond geometries, and can be used to estimate the amount of symmetric or distorted coordination shells. It must be clarified why the spectrum averaged over the HCTH407 sampling, as well as the six spectra of Fig. 11, have more in common with the DD-DA and the DD-SA spectra rather than with those generated from undercoordinated oxygens. This, in spite of the fact that, according to the H-bond definition used in this work, in most of the selected instantaneous configurations, the amount of DD-DA molecules is lower than 50%. One reason is that in the box of 32 molecules, even if

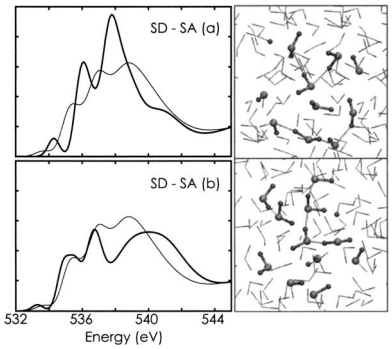

FIG. 15. XAS of two O atoms which have been identified as SD-SA following the H-bond definition in Ref. 5. The configuration around each O is displayed in the right panels, where the atoms within a distance of 4 Å from the absorbing oxygen are depicted as balls, whereas the farther molecules are rendered by simple lines.

less than 16 are DD-DA, most of them are at least DD or DA. Moreover, the H-bond criterion used here is rather restrictive, as already recognized by Odelius *et al.*[45] It selects quite strong H-bond interactions. We noticed, for example, that there are molecules identified as SA-SD, which still interact with one or two more molecules through "highly distorted" H bonds. An example for this situation is given in Fig. 15, where the contrast between two different SD-SA molecules is proposed. Despite the fact that the two configurations (a) and (b) are both identified as SD-SA, the corresponding absorption spectra are rather different. In case (a), the molecule is connected by two almost linear H bonds with lengths of 3.3 and 2.8 Å, respectively. The next closest O atoms are at 3.2 and 3.3 Å, but the H-bond angles are 57° and 32°, respectively, resulting in very weak interactions. Configuration (b), instead, is characterized by two relatively strong H bonds, at 2.62 and 2.78 Å, with angles of about 20°, plus at least one more moderate interaction on the accepting side. The corresponding O–O distance is 3.1 Å and the bending angle is 30°. This latter interaction seems to be sufficient to determine the rehybridization of the lone pair, and can be counted as a weak H bond. As a result, the postedge band is filled, while the main edge is partially quenched. The fore peak, indicating the presence of broken H bonds of donor type, instead, is still present. Conditions, such as the ones just described, are most probably associated with processes of formation or breaking of bonds. Therefore, a certain degree of rehybridization and charge redistribution is still present and the corresponding XA spectrum may have important contributions in the postedge region as well. It would be necessary to run longer MD trajectories, possibly using larger simulation cells, to improve the statistical sampling of all possible configurations and obtain better balanced spectra. These are computationally demanding calculations that go beyond the scope of this work.

V. CONCLUSIONS

Inner-shell spectroscopy calculations of bulk hexagonal ice and liquid water have been carried out by applying the recently developed technique based on the GAPW formalism. One important advantage of our method over previous x-ray spectroscopy calculations in condensed matter is the

possibility to use the supercell approach together with the full potential scheme. By all-electron calculations performed under PBC, possible finite size effects as well as the role of the basis set representation have been thoroughly investigated. Moreover, the oscillator strengths are computed directly from the extended wavefunctions, without introducing additional approximations, as pseudopotentials or frozen cores.

The calculations performed on the well known structure of bulk ice demonstrate the reliability of the technique. It has been verified that, also for extended systems, sufficiently large basis sets are required to provide the necessary flexibility in the description of the empty states contributing to the spectral distribution. Moreover, it has been observed that, even if x-ray absorption is a local process, it is important to describe correctly the extended character of the wavefunction in condensed matter systems. Too small simulation cells or limited QM regions, in the case of QM/MM calculations, produce overstructured spectra that might be misinterpreted. Concerning the choice of the core-hole potential, HCH turns out to be superior with respect to FCH. The latter, indeed, induces strong deformations of the spectral profile, which diverges substantially from the experimental curve. XFCH, on the other hand, partially corrects the FCH misbehavior. The main features of the ice spectrum can be recognized in the XFCH curve, even if the postedge oscillator strengths are still shifted downward by more than 2.5 eV, resulting in the shrinking of the stepwise structure and in an overall too compact shape.

The second part of the work is focused on the more complex case of liquid water and on the relationship between the structure of the H-bond network and the resulting XAS. Spectra averaged over MD trajectories, as well as spectra obtained from single snapshots, or even from one single absorbing oxygen, have been compared to single out the effects of specific atomic environments. Also, in this case, different basis sets and different core-hole potentials have been tested. From the numerous calculations carried out, we conclude that our simulation technique is indeed sensitive to variations in the coordination of the O atoms. Single-snapshot spectra show that specific features appear by variations of the number of DD and DA. Similar trends are obtained by using either HCH or XFCH, even if the best choice in terms of agreement with experiment is again the half-core formalism. The signature of asymmetric coordination shells could be identified by the direct comparison of spectra generated for specific structures with different amounts of DD-DA oxygens. Our results confirm, as suggested in previous works,[2,6,17] that the formation of the pre-edge structure in liquid water XAS, as well as the reshaping of the main and postedge bands, can be attributed to changes in the rehybridization of the molecular orbitals due to the fluctuations of H bonds. However, it has also been observed that the spectra obtained from the trajectories analyzed here are still dominated by contributions associated with the formation of H bonds and the consequent charge redistribution. In particular, the spectra generated from individual O atoms show that hydrogen bonding effects and the resulting orbital rehybridization are often still relevant even for strongly distorted geometries. The presence of these weak H-bond interactions, associated with processes of formation or breaking of bonds, contributes to the postedge band. The corresponding oscillator strengths remain localized in a limited energy interval and form a compact band with a maximum, in place of the broad distribution of experiment. Therefore, the plain counting of H bonds, by choosing a geometrical criterion, to describe the properties of the liquid structure seems to be not adequate.

In conclusion, it has been demonstrated that our method for condensed matter calculations of x-ray absorption spectra is able to resolve structural changes in hydrogen bonded systems. Since the interpretation of experimental spectra of complex structures is not always straightforward, such a tool can be helpful in better understanding the links between spectral signatures and specific atomic environments. In the present work, these links have been discussed for the case of liquid water and a picture of how distortions of the H-bond network affect the spectrum has been provided. Some discrepancies with the experimental findings still remain, though. For further improvement in the description of liquid water, it would be necessary to run longer trajectories for larger samples, in order to generate better statistical samplings of the oxygen environment. It would also be instructive to apply x-ray spectroscopy techniques to path-integral trajectories, thus including quantum effects on the structure and dynamics of the H-bond network into the calculation of the spectral profile. To our knowledge, this sort of path-integral XAS simulations has not been carried out yet. However, the entailed additional work is very much computer intensive and goes beyond the present scope.

ACKNOWLEDGMENTS

I wish to thank Professor J. Hutter for his scientific support and for the fruitful discussions and the University of Zurich for the financial support. I would also like to acknowledge Dr. J. VandeVondele and Dr. T. Teodorova, who provided the MD trajectories, and the Swiss Center for Scientic Computing (CSCS) for the computational support.

[1] A. Nilsson and L. G. M. Pettersson, Surf. Sci. Rep. **55**, 49 (2004).
[2] S. Myneni, Y. Luo, L. Å. Näslund, M. Cavalleri, L. Ojamäe, H. Ogasawara, A. Palmenschikov, P. Wernet, P. Väterlaein, C. Heske, Z. Hussain, L. G. Pettersson, and A. Nilsson, J. Phys.: Condens. Matter **14**, 213 (2002).
[3] K. R. Wilson, M. Cavalleri, B. Rude, R. Schaller, A. Nilsson, L. G. M. Pettersson, N. Goodman, T. Catalano, J. Bozek, and R. J. Saykally, J. Phys.: Condens. Matter **14**, L221 (2002).
[4] K. R. Wilson, M. Cavalleri, B. Rude, R. Schaller, T. Catalano, A. Nilsson, R. J. Saykally, and L. G. M. Pettersson, J. Phys. Chem. B **109**, 10194 (2005).
[5] M. Iannuzzi and J. Hutter, Phys. Chem. Chem. Phys. **9**, 1599 (2007).
[6] P. Wernet, D. Nordlund, U. Bergmann, M. Cavalleri, M. Odelius, H. Ogasawara, L. Å. Näslund, T. K. Hirsch, L. Ojamäe, P. Glatzel, L. G. M. Pettersson, and A. Nilsson, Science **304**, 995 (2004).
[7] D. Nordlund, H. Ogasawara, P. Wernet, M. Nyberg, M. Odelius, L. G. M. Pettersson, and A. Nilsson, Chem. Phys. Lett. **395**, 161 (2004).
[8] M. Leetmaa, T. Wikfeldt, M. Ljungberg, M. Odelius, J. Swenson, A. Nilsson, and L. G. M. Pettersson, J. Chem. Phys. (unpublished).
[9] F. Paesani, W. Zhang, D. A. Case, T. E. Cheatham, and G. A. Voth, J. Chem. Phys. **125**, 184507 (2006).
[10] F. Paesani, S. Iuchi, and G. A. Voth, J. Chem. Phys. **127**, 074506 (2007).
[11] J. Grossman, E. Schwegler, E. Draeger, F. Gygi, and G. Galli, J. Chem.

Phys. **120**, 300 (2004).
[12] J. Grossman, E. Schwegler, and G. Galli, J. Phys. Chem. B **108**, 15865 (2004).
[13] E. Schwegler, J. Grossman, F. Gygi, and G. Galli, J. Chem. Phys. **121**, 5400 (2004).
[14] I.-F. Kuo, C. J. Mundy, M. J. McGrath, J. I. Siepmann, J. VandeVondele, M. Sprik, J. Hutter, B. Chen, M. L. Klein, F. Mohamed, M. Krack, and M. Parrinello, J. Phys. Chem. B **108**, 12990 (2004).
[15] J. VandeVondele, F. Mohamed, M. Krack, J. Hutter, M. Sprik, and M. Parrinello, J. Chem. Phys. **122**, 014515 (2005).
[16] W. Kohn and L. J. Sham, Phys. Rev. **140**, A1133 (1965).
[17] M. Cavalleri, M. Odelius, A. Nilsson, and L. G. M. Pettersson, J. Chem. Phys. **121**, 10065 (2004).
[18] B. Hetenyi, F. D. Angelis, P. Giannozzi, and R. Car, J. Phys. Chem. B **120**, 8632 (2004).
[19] M. Cavalleri, M. Odelius, D. Nordlund, A. Nilsson, and L. G. M. Pettersson, Phys. Chem. Chem. Phys. **7**, 2854 (2005).
[20] D. Prendergast and G. Galli, Phys. Rev. Lett. **96**, 215502 (2006).
[21] R. Wang, H. Kreuzer, and M. Grunze, Phys. Chem. Chem. Phys. **8**, 4744 (2006).
[22] B. Hetenyi, F. D. Angelis, P. Giannozzi, and R. Car, J. Chem. Phys. **115**, 5791 (2001).
[23] M. Iannuzzi, T. Chassaing, T. Wallman, and J. Hutter, Chimia **59**, 499 (2005).
[24] J. VandeVondele, M. Iannuzzi, and J. Hutter, Lect. Notes Phys. **703**, 287 (2006).
[25] CP2K a general program to perform molecular dynamics simulations, 2007 (http://cp2k.berlios.de/).
[26] L. Triguero, L. G. M. Pettersson, and H. Ågren, Phys. Rev. B **58**, 8097 (1998).
[27] A. D. Becke, Phys. Rev. A **38**, 3098 (1988).
[28] C. T. Lee, W. T. Yang, and R. G. Parr, Phys. Rev. B **37**, 785 (1988).
[29] In this work, three different classes of all electron basis sets are used: the Pople basis sets (Ref. 30), of the type 6-311G, the Dunning basis sets (Ref. 31), such as aug-cc-pVQZ, the IGLO-III basis sets (Ref. 32).
[30] R. Krishnan, J. Binkley, R. Seeger, and J. Pople, J. Chem. Phys. **72**, 650 (1980).
[31] T. H. Dunning, J. Chem. Phys. **90**, 10073 (1989).
[32] W. Kutzelnigg, U. Fleischer, and M. Shindler, *NMR-Basic Principles and Progress* (Springer-Verlag, Heidelberg, 1990), Vol. 23.
[33] A. Nilsson, H. Ogasawara, M. Cavalleri, D. Nordlund, M. Nyberg, P. Wernet, and L. G. M. Pettersson, J. Chem. Phys. **122**, 154505 (2005).
[34] M. Cavalleri, H. Ogasawara, L. G. M. Pettersson, and A. Nilsson, Chem. Phys. Lett. **364**, 363 (2002).
[35] D. Nordlund, H. Ogasawara, H. Bluhm, O. Takahashi, M. Odelius, M. Nagasono, L. G. M. Pettersson, and A. Nilsson, Phys. Rev. Lett. **99**, 217406 (2007).
[36] T. Laino, F. Mohamed, A. Laio, and M. Parrinello, J. Chem. Theory Comput. **1**, 1176 (2005).
[37] P. Blöchl, J. Chem. Phys. **102**, 7422 (1995).
[38] W. Jorgensen, J. Chem. Phys. **77**, 4156 (1982).
[39] D. Asthagiri, L. R. Pratt, and J. D. Kress, Phys. Rev. E **68**, 041505 (2003).
[40] A. D. Becke, J. Chem. Phys. **98**, 5648 (1993).
[41] F. Hamprecht, A. Cohen, D. Tozer, and N. C. Handy, J. Chem. Phys. **109**, 6264 (1998).
[42] A. D. Boese and N. C. Handy, J. Chem. Phys. **114**, 5497 (2001).
[43] S. Goedecker, M. P. Teter, and J. Hutter, Phys. Rev. B **54**, 1703 (1996).
[44] T. Teodorova, A. Seitsonen, J. Hutter, I.-F. Kuo, and C. J. Mundy, J. Phys. Chem. B **110**, 3685 (2006).
[45] M. Odelius, M. Cavalleri, A. Nilsson, and L. G. M. Pettersson, Phys. Rev. B **73**, 024205 (2006).